Ultraviolet and Optical Flare from the Tidal Disruption of a Helium-Rich Stellar Core

S. Gezari[1,11], R. Chornock[2], A. Rest[3], M. E. Huber[4], K. Forster[5], E. Berger[2], P. J. Challis[2], J. D. Neill[5], D. C. Martin[5], T. Heckman[1], A. Lawrence[6], C. Norman[1], G. Narayan[2], R. J. Foley[2,12], G. H. Marion[2], D. Scolnic[1], L. Chomiuk[2], A. Soderberg[2], K. Smith[7], R. P. Kirshner[2], A. G. Riess[1], S. J. Smartt[7], C.W. Stubbs[2], J.L. Tonry[4], W. M. Wood-Vasey[8], W. S. Burgett[4], K. C. Chambers[4], T. Grav[9], J. N. Heasley[4], N. Kaiser[4], R.-P. Kudritzki[4], E. A. Magnier[4], J. S. Morgan[4], & P. A. Price[10]

[1]*Department of Physics and Astronomy, Johns Hopkins University, 3400 North Charles Street, Baltimore, MD 21218, USA.*

[2]*Harvard-Smithsonian Center for Astrophysics, 60 Garden Street, Cambridge, MA 02138, USA.*

[3]*Space Telescope Science Institute, 3700 San Martin Drive, Baltimore, MD 21218, USA.*

[4]*Institute for Astronomy, University of Hawaii, 2680 Woodlawn Drive, Honolulu HI 96822, USA.*

[5]*California Institute of Technology, 1200 East California Blvd., Pasadena, CA 91125, USA.*

[6]*Institute for Astronomy, University of Edinburgh Scottish Universities Physics Alliance, Royal Observatory, Blackford Hill, Edinburgh, EH9 3HJ, UK.*

[7]*Astrophysics Research Centre, School of Mathematics and Physics, Queen's University Belfast, Belfast, BT7 1NN, UK.*

[8]*Pittsburgh Particle Physics, Astrophysics, and Cosmology Center, Department of Physics and Astronomy, University of Pittsburgh, 3941 O'Hara Street, Pittsburgh, PA 15260, USA.*

[9]*Planetary Science Institute, 1700 East Fort Lowell, Tucson, AZ 85719, USA*

[10]*Department of Astrophysical Sciences, Princeton University, Princeton, NJ 08544, USA.*

[11]*Hubble Fellow.*

[12]*Clay Fellow.*

The flare of radiation from the tidal disruption and accretion of a star can be used as a signpost for supermassive black holes that otherwise lie dormant in the centres of distant galaxies[1]. Previous candidate flares[2–6] have demonstrated declining light curves in good agreement with expectations, but with poor constraints on the time of disruption and the type of star disrupted, because they did not see the rising emission. Recently, two "relativistic" candidate tidal disruption events were discovered whose extreme X-ray luminosities ($L_X \sim 10^{47}$ ergs s^{-1}) and synchrotron radio emission were interpreted as the onset of emission from a relativistic jet [7–10]. Here we report the discovery of a luminous ultraviolet and optical flare from the nuclear region of an inactive galaxy at $z = 0.1696$. The observed continuum is cooler than expected for a simple accreting debris disk, but the well-sampled rise and decline of its light curve follows the predicted mass accretion rate, and can be modeled to determine the time of disruption to an accuracy of two days, with a black hole mass of $\sim 2 \times 10^6$ solar masses, modulo a factor dependent on the mass and radius of the star disrupted. We determine that the disrupted star was a helium-rich stellar core, based upon the spectroscopic signature of ionised helium from the unbound debris.

When the pericenter of a star's orbit ($R_{\rm p}$) passes within the tidal disruption radius of a massive black hole, $R_{\rm T} \approx R_\star (M_{\rm BH}/M_\star)^{1/3}$, tidal forces overcome the binding energy of the star, with roughly half of the stellar debris remaining bound to the black hole, while the rest is unbound with high velocities[1]. For black holes above a critical mass, $M_{\rm crit} \approx 10^8 r_\star^{3/2} m_\star^{-1/2} M_\odot$ where $r_\star = R_\star/R_\odot$ and $m_\star = M_\star/M_\odot$, the star is captured by the event horizon of the black hole before being disrupted. The mass accretion rate ($\dot{M}$) in a tidal disruption event (TDE) can be calculated directly from the orbital return-times of the bound debris[1,11,12]. For the simplest case of a star of uniform density this yields, $\dot{M} = (2/3)(fM_\star/t_{\rm min})(t/t_{\rm min})^{-5/3}$, where f is the fraction of the star accreted and $t_{\rm min}$ is the orbital period of the most tightly bound debris and the time delay between the time of disruption and the start of the flare, and scales as $M_{\rm BH}^{1/2} M_\star^{-1} R_\star^{3/2}$ for $R_{\rm p} = R_{\rm T}$. The radiative output of the accreted debris is less certain, and depends on the ratio of the accretion rate to the Eddington rate[13].

The optical transient, PS1-10jh ($\alpha_{\rm J2000} = 242.3679, \delta_{\rm J2000} = +53.6732$), was discovered on 2010 May 31.45 UT in the Pan-STARRS1[14] Medium Deep Survey (PS1 MDS) by our two independent image differencing pipelines. The densely sampled ($\Delta t \sim 3$ d) optical $g_{\rm P1}$, $r_{\rm P1}$, $i_{\rm P1}$, and $z_{\rm P1}$ light curve of PS1-10jh follows the rise of the transient to its peak in the $g_{\rm P1}$ band on 2010 July 12.31 UT and its subsequent decline until 2011 September 1.24 UT (Supplementary Table 1). PS1-10jh was discovered independently as a transient NUV source at the 20σ level by the *GALEX*[15] Time Domain Survey (TDS) on 2010 June 17.68 UT within 2.5 ± 3.0 arcsec, and was detected in 10 more epochs of TDS observations through 2011 June 10.68 UT (Supplementary Table 2). No source is detected in a deep coadd of all the TDS epochs in 2009, with a 3σ upper limit of > 25.6 mag implying a peak amplitude of variability in the NUV of > 6.4 mag. See the Supplementary Information for details on the PS1 and *GALEX* photometry.

PS1-10jh is coincident with the center of a galaxy within the 3σ positional uncertainty of 0.036 arcsec (Supplementary Information) with rest-frame u, g, r, i, and z photometry from SDSS[16] and K photometry from UKIDSS[17] fitted with a galaxy template[18] with $M_{stars} = (3.6 \pm 0.2) \times 10^9 M_\odot$ and $M_{\rm r} = -18.7$ mag. The central black hole mass determined indirectly from locally established scaling relations[19] is $4^{+4}_{-2} \times 10^6 M_\odot$. We obtained 5 epochs of optical spectroscopy at the location of PS1-10jh between 2010 June 16.33 and 2011 September 4.23 UT with the 6.5-m MMT (Supplementary Table 3). The continua in the spectra are well modeled by the combination of a galaxy host at $z = 0.1696$ ($d_L = 816$ Mpc) with a stellar population with an age of $1.4 - 5.0$ Gyr, depending on the chosen metallicity, and a fading hot blackbody component with $T_{\rm BB} \sim 3 \times 10^4$ K (Fig. 1).

The spectra show no narrow emission lines that would be indicative of star formation or an active galactic nucleus (AGN). We obtained a 10 ks *Chandra* DDT $0.2 - 10$ keV X-ray observation at the location of PS1-10jh on 2011 May 22.96 UT, and detected no source above the background with a 3σ upper limit of $L_X(0.2 - 10$ keV$) < 5.8 \times 10^{41}$ ergs s^{-1} for an unobscured AGN spectrum. The X-ray faintness and extreme NUV variability amplitude of PS1-10jh, and its prolonged brightness in the ultraviolet, strongly disfavor an AGN or supernova origin, respectively

(Supplementary Information).

The rise and decay of the light curve of PS1-10jh is well described by numerical simulations for the mass return-rate from a star that is tidally disrupted at $R_{\mathrm{p}} = R_{\mathrm{T}}$ with an internal structure parameterised by a polytropic exponent of $5/3$ characteristic of a fully convective star or a degenerate core[20] (Fig. 2). The decline from the peak is too steep to be fitted by simulations for a more centrally concentrated stellar structure, such as one characteristic of a solar-type star (Supplementary Information). There are systematic differences between the light curve and the model during the early rise (earlier than -44 rest-frame days from the peak) and the late decay (later then 240 rest-frame days from peak) which could imply a stellar structure more complex than one described by a single polytrope. The mass of the black hole is determined from the stretch factor of 1.38 ± 0.03 applied to fit the model for a $10^6 M_\odot$ black hole to the light curve, which implies a time of disruption of 76 ± 2 d before the peak and $M_{\mathrm{BH}} = (1.9 \pm 0.1) \times 10^6 m_\star^2 r_\star^{-3} M_\odot$.

The most constraining property of PS1-10jh is the detection of very broad high-ionisation He II$\lambda 4686$ (FWHM $= 9{,}000 \pm 700$ km s^{-1}) and $\lambda 3203$ lines that fade in time along with the ultraviolet and optical continuum. The lack of Balmer line emission in the spectra requires an extremely low hydrogen mass fraction of < 0.2 (Supplementary Information), which cannot be found in the ambient interstellar medium or in a passive accretion disk. This is the strongest evidence that PS1-10jh must be fueled by the accretion of a star that has lost its hydrogen envelope, either through stellar winds or tidal interactions with the central SMBH. The broad width of the line is also what one expects from the velocities of the most energetic unbound stellar debris in a TDE[21], $v_{\max} \sim 1 \times 10^4 (M_{\mathrm{BH}}/10^6 M_\odot)^{1/6} (R_{\mathrm{T}}/R_{\mathrm{p}}) r_\star^{-1/2} m_\star^{1/3}$ km s^{-1}.

We measure the SED of the flare over time from the nearly simultaneous PS1 optical and *GALEX* ultraviolet observations (with the host galaxy flux removed) (Fig. 3). The pre-peak SED is fitted by a blackbody with $T_{\mathrm{BB}} = (2.9 \pm 0.2) \times 10^4$ K, consistent with the blackbody component seen in the spectra. However, the temperature fit is very sensitive to internal extinction. If we correct for the maximum internal extinction of $E(B - V) = 0.08$ mag allowed by the observed He II$\lambda 3203/4686$ ratio, the best-fit temperature increases to $(5.5 \pm 0.4) \times 10^4$ K. In fact, we know that the photoionising continuum must have $T_{\mathrm{BB}} \gtrsim 5 \times 10^4$ K at 22 rest-frame days before the peak in order to produce enough $\lambda < 228$ Å photons to photoionise the He II$\lambda 4686$ line observed with a luminosity of $(9 \pm 1) \times 10^{40}$ ergs s^{-1}. The late-time SED can be fitted with the same temperature as the pre-peak SED. Note that the observed continuum temperature, and even the maximum temperature allowed by possible de-reddening, are considerably cooler than the temperature of $\approx 2.5 \times 10^5 (M_{\mathrm{BH}}/10^6 M_\odot)^{1/12} r_\star^{-1/2} m_\star^{-1/6}$ K expected from material radiating at the Eddington limit at the tidal radius[13]. This discrepency is also seen in AGN[22] and may imply that the continuum we see is due to reprocessing of some kind[22,23]

Based on the arguments above, we assume that the observed temperature is a lower limit, $T_{\mathrm{BB}} \gtrsim 3 \times 10^4$ K, and thus the peak bolometric luminosity is $\gtrsim 2.2 \times 10^{44}$ ergs s^{-1}, and the total

3

energy emitted from integrating under the light-curve model is $\gtrsim 2.1 \times 10^{51}$ ergs, corresponding to a total accreted mass (M_{acc}) of $\gtrsim 0.012(\epsilon/0.1)^{-1}M_\odot$, where ϵ is the efficiency of converting matter into radiation.

The internal structure and helium-rich abundance of the star derived from the light curve and the spectra can be consistently modeled by the tidally stripped core of a Red Giant (precursor to a helium white dwarf) that had a main sequence mass of $M_\star \gtrsim 1M_\odot$ in order to have evolved off the main sequence in less time than the age of the stellar population (< 5 Gyr). This tidal stripping mechanism has been invoked to explain the hot stars in the Galactic Center[24], and the rate of tidal disruption of tidally stripped stars is likely to be higher than solar-type stars[25]. The mass of the black hole from the light curve fit depends on the mass and radius of the star at the time of disruption. Using $M_\star \sim 0.23M_\odot$ and $R_\star \sim 0.33R_\odot$ measured for a Red Giant core that was stripped in a binary system[26], assuming that the evolution of the core is similar to one that is tidally stripped, one gets $f = M_{\mathrm{acc}}/M_\star \gtrsim 0.058$, approaching the $f \gtrsim 0.1$ measured in simulations[27], $M_{\mathrm{BH}} = (2.8 \pm 0.1) \times 10^6 M_\odot$, and a peak luminosity approaching the Eddington luminosity of the SMBH ($L_{\mathrm{peak}} \gtrsim 0.6L_{\mathrm{Edd}}$).
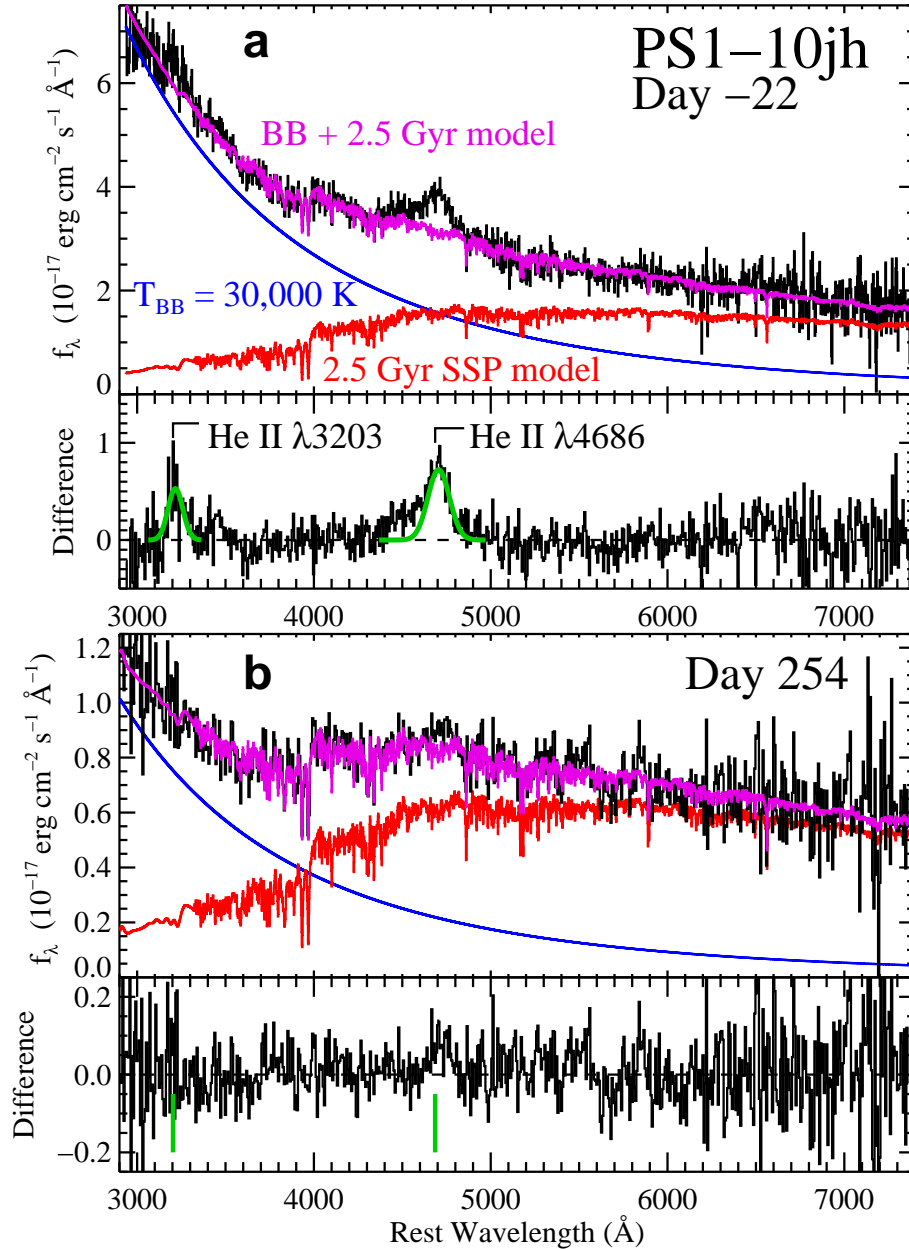
Figure 1

Optical spectrum. MMT optical spectrum of PS1-10jh obtained -22 (**a**) and $+254$ (**b**) rest-frame days from the peak. The continuum is fitted with a combination of a stellar population of 2.5 Gyr and a fading blackbody with a temperature of $\sim 3 \times 10^4$ K determined from the UV and optical spectral energy distribution. He IIλ 4686 (Fowler series $n = 4 \to 3$) is detected above the continuum, and fitted with a Gaussian with a FWHM = $(9,000 \pm 700)$ km s^{-1} and $L = (9 \pm 1) \times 10^{40}$ ergs s^{-1} (plotted with a green line in the early epoch). Residual emission above the galaxy plus blackbody model is also detected at ~ 3200 Å which is coincident with the location of the He IIλ3203 (Fowler series $n = 5 \to 3$) line, and confirms the identification of He IIλ4686. The observed flux ratio of He II

5

$\lambda 3203/\lambda 4686 = 0.50 \pm 0.10$, measured with a Gaussian fit to the He II $\lambda 3203$ line with a width fixed to that of He II $\lambda 4686$, limits the internal extinction to $E(B - V) < 0.08$ mag (Supplementary Information). The He II$\lambda 4686$ line is still evident as an excess above the model in the later epoch, however it has faded by a factor of ~ 10 since the pre-preak spectrum, the same factor by which the ultraviolet continuum has faded during this time. Note that the absolute flux scaling in the later epoch is uncertain due to clouds on the date of the observation.
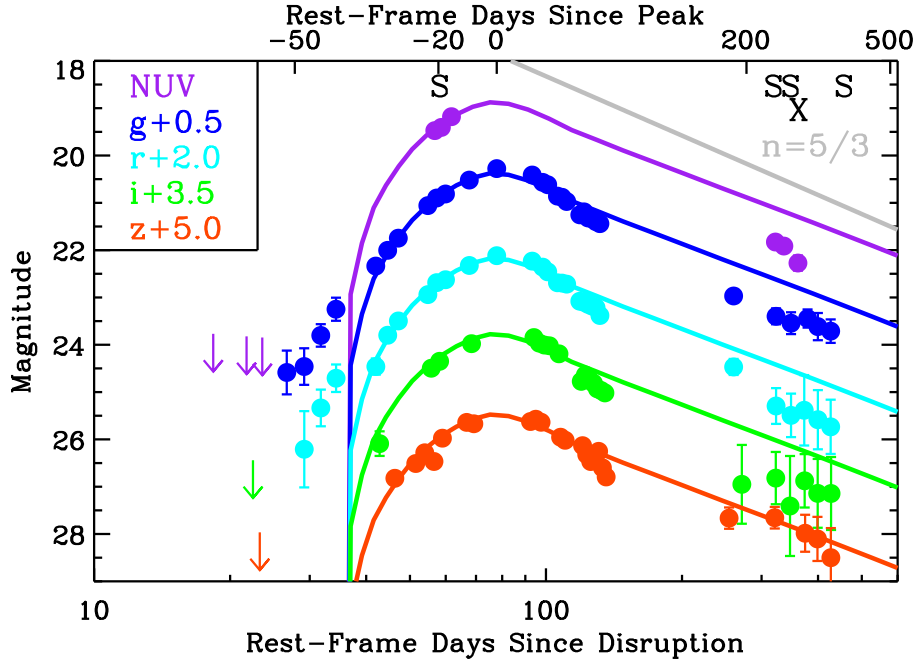

Figure 2

Ultraviolet and optical light curve. The *GALEX NUV* and PS1 g_{P1}-, r_{P1}-, i_{P1}-, and z_{P1}- band light curve of PS1-10jh (with the host galaxy flux removed) with 1σ error bars and in logarithmic days since the peak (top) and since the time of disruption (bottom) determined from the best fit of the g_{P1}-band light curve to the numerical model[20] for the mass accretion rate of a tidally disrupted star with a polytropic exponent of $5/3$ (shown with solid lines scaled to the flux in the *GALEX* and PS1 bands). We performed a least-squares fit of the model for a $10^6 M_\odot$ black hole to the light curve from -36 to 58 rest-frame days from the peak for each of the four optical bands independently with the time of disruption, a vertical scaling factor, and a stretch factor in time as free parameters. The *GALEX* and PS1 photometry at $t > 240$ rest-frame days since the peak is shown binned in time in order to increase the signal-to-noise. The dates of multiple epochs of MMT spectroscopy are marked with an S, and the date of the *Chandra* X-ray observation is marked with an X. Grey line shows an $n = 5/3$ power-law decay from the peak. Arrows show 3σ upper limits.
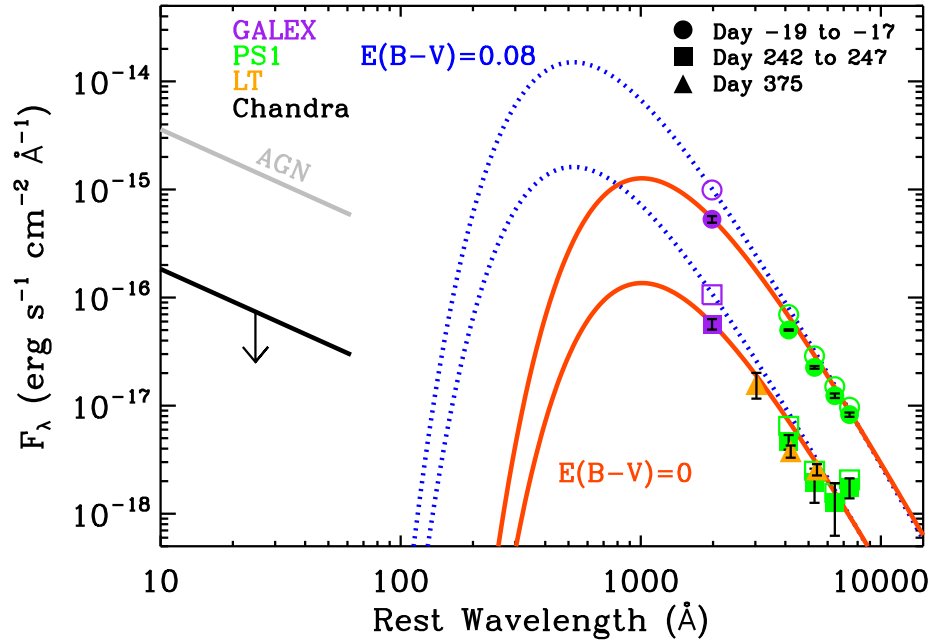
Figure 3

Spectral energy distribution. Spectral energy distribution of PS1-10jh during nearly simultaneous *GALEX* ultraviolet and PS1 optical observations (with the host galaxy flux removed) at two epochs, with 1σ error bars and labeled by their time in rest-frame days from the peak of the flare. Flux densities have been corrected for Galactic extinction of $E(B-V) = 0.013$ mag. The ultraviolet and optical SED from -19 to 247 d is fitted with a 2.9×10^4 K blackbody. Orange solid lines show blackbodies with this temperature scaled to the NUV flux density. Open symbols show the *GALEX* and PS1 flux densities corrected for an internal extinction of $E(B-V) = 0.08$ mag, and dotted blue line shows the 5.5×10^4 K blackbody fit to the de-reddened flux densities. The upper limit from the Chandra DDT observation on 2011 May 22.96 UT assuming a $\Gamma = 2$ spectrum typical of an AGN is plotted with a thick black line. The X-ray flux density expected from an unobscured AGN with a comparable NUV flux is plotted for comparison with a thick grey line[28]. Also shown are the u, g, and r band flux densities measured from aperture photometry with the Liverpool Telescope[29] on 2011 Sep 24 UT, after subtracting the host galaxy flux measured by SDSS.

Contributions   S.G. designed the observations and the transient detection pipeline for *GALEX* TDS, and measured the UV photometry of PS1-10jh. K.F. and J.D.N coordinated, and D.C.M. facilitated the *GALEX* TDS observations. A.R. designed the `photpipe` transient detection pipeline hosted by Harvard/CfA for PS1 MDS, and measured the optical photometry of PS1-10jh. R.C. designed, implemented, and analysed the MMT optical spectroscopy observations, and contributed to the operation of `photpipe` and the visual inspection of transient alerts. E.B. proposed for and facilitated the MMT observations. M.H., G.N., D.S., and R.J.F. contributed to the operation of `photpipe` and the visual inspection of transient alerts. P.J.C., R.J.F., G.H.M., L.C., and A.S. contributed to the MMT observations. S.S. designed, and K.S. operated, the transient pipeline for PS1 MDS hosted by Queen's Belfast. C.W.S., J.L.T., and W.M.W.-V. facilitated the transient pipelines for PS1 MDS. W.B., K.C.C., T.G., J.N.H., N.K., R.-P.K., E.A.M., J.S.M., P.A.P., C.W.S., and J.L.T. are builders of the PS1 system. S.G. requested the DDT *Chandra* X-ray observation and analysed the data. A.L. obtained the Liverpool Telescope optical imaging observations and analysed the data, and stimulated discussions on the nature of the SED of PS1-10jh. S.G. analysed and modelled the multi-colour light curve and the SED of PS1-10jh. T.H. and C.N. stimulated discussions on the nature of the star disrupted. The paper was put together and written by S.G., and all authors provided feedback on the manuscript.

Author Information   Reprints and permissions information is available at www.nature.com/reprints. The authors declare no competing financial interests. Correspondence and requests for materials should be addressed to S.G. (email: suvi@pha.jhu.edu).

SUPPLEMENTARY INFORMATION

1 Pan-STARRS1 Medium Deep Survey Observations

The Pan-STARRS1 system (PS1) is a high-etendue wide-field imaging system designed for dedicated survey observations, on a 1.8 meter telescope on Haleakala with a 1.4 Gigapixel camera and a 7 deg^2 field of view[14]. The PS1 observations are obtained through a set of five broadband filters, which we have designated as g_{P1} ($\lambda_{eff} = 483$ nm), r_{P1} ($\lambda_{eff} = 619$ nm), i_{P1} ($\lambda_{eff} = 752$ nm), z_{P1} ($\lambda_{eff} = 866$ nm), and y_{P1}($\lambda_{eff} = 971$ nm). Although the filter system for PS1 has much in common with that used in previous surveys, such as SDSS[16], there are important differences. The g_{P1} filter extends 20 nm redward of g_{SDSS}, paying the price of 5577Å sky emission for greater sensitivity and lower systematics for photometric redshifts, and the z_{P1} filter is cut off at 930 nm, giving it a different response than the detector response defined z_{SDSS}. SDSS has no corresponding y_{P1} filter.

This paper uses images and photometry from the PS1 Medium-Deep Field survey (MDS). The PS1 MDS obtains deep multi-epoch images in the g_{P1}, r_{P1}, i_{P1}, z_{P1} and y_{P1} bands of 10 fields distributed across the sky chosen for their overlap with extragalactic legacy survey fields with multiwavelength corollary data. The typical Medium-deep cadence of observations cycles through the g_{P1}, r_{P1}, i_{P1} and z_{P1} bands every 3 nights, with observations in the y_{P1} band close to the full moon. Images are processed through the Image Processing Pipeline (IPP[30]), which runs the images through a succession of stages, including flat-fielding ("de-trending"), a flux-conserving warping to a sky-based image plane, masking and artifact removal, and object detection and photometry. The 8 images taken during any one night are stacked to produce a "nightly stack". This nightly data product is used in two image differencing pipelines which run simultaneously, but independently.

In this paper, we present photometry from the `photpipe` pipeline hosted at Harvard/CfA[31]. This pipeline produces image differences from the nightly stacks and image difference detections which are published to an alerts webpage for visual inspection if there are 3 associated $> 5\sigma$ detections. Forced-centroid PSF-fitting photometry is applied on its image differences, with a PSF derived from reference stars in each nightly stack. The zeropoints are measured for the AB system from comparison with field stars in the SDSS catalog. The photometry is in the natural PS1 system, $m = -2.5 \log(flux) + m'$, with a single zerpoint adjustment m' made in each band to conform to the AB magnitude scale, with an accuracy of better than 1%. We do not include the y_{P1} band photometry which has an additional uncertainty of ~ 0.05 mag in the zeropoint due to the lack of an SDSS comparison. We propagate the poisson error through the resampling and image differencing. In order to correct for covariance, we do forced photometry in apertures at random positions, calculate the standard deviation of the ratio between the flux and the error, and multiply our errors by this value. Nightly image differences yield 3σ limiting magnitudes of ~ 23.5 mag in g_{P1}, r_{P1}, i_{P1}, and $z_{P1}$and a typical positional accuracy of ~ 0.5 pixels (0.1 arcsec) which depends on the S/N and FWHM of the source. The deep template used for the image differencing of PS1-10jh includes the transient flux, and so we also subtract off a negative baseline flux, which

is measured from the epochs before the start of the flare in 2009. We add the error in the mean baseline flux to the photometric error in quadrature. The image differencing photometry for PS1-10jh is reported in AB magnitudes in Table S1. In order to improve the signal-to-noise (S/N) in the photometry at late-times ($t > 240$ rest-frame days after the peak) in the figures, we binned the data into time intervals of 30 days.

We measure the positional offset between the transient PS1-10jh and the centroid of its host galaxy measured from the nightly stacks before the event. Figure S4 shows the offset in x and y from the mean position of the host galaxy before the event. The resulting offset during the event is within the 3σ uncertainty of 0.18 pixels (0.036 arcsec), plotted with a thick gray circle.

The PS1 system is developing the Transient Science Server (TSS) which automatically takes the nightly stacks, creates image differences with reference images created from deep stacks, carries out PSF fitting photometry on the image differences, and returns catalogues of variable and transient candidates. Photometric and astrometric measurements are performed by the IPP system[32, 33]. Individual detections made on the image differences are currently ingested into a MySQL database hosted at Queen's University Belfast after an initial culling of objects based on the detection of saturated, masked or suspected defective pixels within the PSF area. Sources detected on the nightly image differences are assimilated into potential real astrophysical transients based on a set of quality tests. Transient candidates which pass this automated filtering system are promoted for human screening, which currently runs at around 10% efficiency (i.e. 10% of the transients promoted automatically are judged to be real after human screening). Real transients are crossmatched with all available catalogues of astronomical sources in the MDS fields (e.g. SDSS, GSC, 2MASS, APM, Veron AGN, X-ray catalogues) in order to have a first pass classification of supernovae, variable star, AGN and nuclear transients.

2 GALEX Time Domain Survey Observations

The *GALEX* Time Domain Survey (TDS[34]) regularly monitored 6 of the 10 PS1 MDS fields in the NUV ($\lambda_{\text{eff}} = 231.6$ nm[35]), with 7 *GALEX* pointings each with a field of view of ~ 1 deg^2 to cover the full PS1 field of view. The observations were taken with a cadence of 2 days during the window of observing visibility of each field (from $2 - 4$ weeks, $1 - 2$ times per year) from April 2009 to June 2011 UT, and a typical exposure time per epoch of 1.5 ks for a 3σ limiting magnitude of $m_{AB} \sim 23.9$ mag. Variable sources are identified as those which demonstrate an amplitude of variability in any epoch of $> 5\sigma$ from the mean aperture magnitude, where σ is determined empirically as a function of magnitude for each epoch from the standard deviation of reference stars in the images. PS1-10jh was discovered independently from PS1 as a transient NUV source at the 20σ level at RA 242.3685 Dec +53.6738 (J2000) on 2010 June 17.68 UT. The source was undetected in observations between 2009 May 9.52 and 2010 May 9.86 UT. Figure S5 shows the maximum NUV amplitude of UV variable sources classified as quasars and AGNs from the *GALEX* TDS. PS1-10jh is a clear outlier, its UV variability is more extreme than variability

associated with accretion activity in active galaxies. The *GALEX* photometry is measured with a 6 arcsec radius aperture, and corrected for the energy enclosed by the PSF. The photometry for PS1-10jh is given in AB magnitudes in Table S2. The 1σ error is determined empirically as described above. To improve the S/N in the photometry at late-times ($t > 240$ rest-frame days after the peak) in the figures, we binned the 8 late-time epochs of data into 3 time intervals in 2011 April, May, and June UT.

3 MMT Spectroscopy

We obtained five epochs of optical spectroscopy of PS1-10jh using the Blue Channel[36] and fiber-fed Hectospec[37] spectrographs on the 6.5-m MMT. We used a long 1 arcsec-wide slit on the Blue Channel, while the Hectospec fibers are 1.5 arcsec in diameter. Details of the observations are presented in Table S3. The Hectospec spectrum was processed using the standard pipeline[38] and a flux calibration was applied using archival observations of the standard star BD+28 4211. Basic two-dimensional image processing and extraction of the Blue Channel data were accomplished using standard routines in IRAF. We then used custom IDL routines to apply flux calibrations and remove telluric absorption based on observations of spectrophotometric standard stars obtained at similar airmasses. The absolute flux scales are unreliable due to clouds and variable seeing on several of the nights of observations, but the spectra were obtained at the parallactic angle[39], so the relative spectral shapes should be reliable. The effects of second-order light contamination are apparent in the day 227 Hectospec data at wavelengths $\gtrsim$ 8500 Å, so we have truncated the spectrum. We also combined the day 254 and 255 Blue Channel spectra into a single spectrum, and refer to it as the day 254 spectrum in this paper. Figure S6 shows the series of spectra.

We created a scaled and weighted stack of all of the post-peak spectra to maximize the S/N in the host spectrum, and fitted the galaxy continuum with template galaxy spectra[40] of different metallicities and stellar populations. The redshift of $z = 0.1696 \pm 0.0001$ was determined by cross-correlating with the best-fit templates. Finally, we performed a chi-squared fit of the models plus a 3×10^4 K blackbody spectrum determined from the UV and optical SED fit, excluding the region around He IIλ4686. Simple stellar population (SSP) models with ages in the range 1.4-5Gyr were all in good agreement with the data. The formal best fit was found for a 2.5 Gyr SSP with a 1/5th solar metallicity. However, there is an age-metallicity degeneracy and somewhat younger models at solar metallicity are also a good fit. The best fit template with a solar metallicity was a 12 Gyr model with an exponentially declining (with an e-folding time of 5 Gyr) star-formation history. However, none of the results in the paper are sensitive to which exact model is chosen within the set of good matches. Our spectral resolution (FWHM = 300 km s^{-1}) is not sufficient to measure the velocity dispersion ($\sigma_\star$) of the host galaxy, which would have $\sigma_\star \lesssim 100$ km s^{-1} for a central black hole of $< 10^7 M_\odot$. In Figure S7 we show the spectrum dereddened for an internal extinction of $E(B - V) = 0.08$ mag fitted with the same galaxy template as in Figure 2, but with a hotter $T_{\mathrm{BB}} \sim 5.5 \times 10^4$ K blackbody component. The quality of the fit is the same with or without internal extinction.

11

4 Chandra Observations

We requested a 10 ks DDT observation with *Chandra*[41] ACIS-S which was obtained on 2010 May 22.96 UT. No source was detected, with a 3σ upper limit of $< 9.4 \times 10^{-4}$ cts s^{-1} calculated using Bayesian statistics with the CIAO v4.3 `aprates` routine for a 4 pixel (1.968 arcsec) radius aperture. This corresponds to a flux of $< 7.2 \times 10^{-15}$ ergs s^{-1} cm^{-2} when corrected for Galactic extinction with $N_H = 3.1 E(B-V) 1.8 \times 10^{21}$ cm$^{-2} = 7.2 \times 10^{19}$ cm^{-2} and assuming a $\Gamma = 2$ energy spectrum typical of an unobscured AGN, or $L_X(0.2-10)$keV$< 5.8 \times 10^{41}$ ergs s^{-1}. The upper limit to the α_{ox} ratio using the NUV observation closest in time on 2011 May 12.37 UT with $L_\nu = (4.3 \pm 0.7) \times 10^{27}$ ergs s^{-1} Hz^{-1} (corrected for Galactic extinction) is $\alpha_{\rm ox} = \log[L_\nu(2500\text{Å})/L_\nu(2\text{keV})]/\log[\nu(2500\text{Å})/\nu(2\text{keV})] < (-1.65 \pm 0.03)$, well below the mean for broad-lined AGN of comparable NUV luminosity of $\alpha_{\rm ox} \sim -1.15$ (Steffen et al. 2006).

The non-detection by *Chandra* is consistent with blackbody emission of $\lesssim 2.5 \times 10^5$ K for bolometric luminosities of up to $\sim 10^{44}$ ergs s^{-1}, close to the Eddington luminosity of the central black hole. For higher blackbody temperatures, such as the range observed in the X-ray TDE candidates from *ROSAT*, *XMM-Newton*, and *Chandra*[5] of $6-12 \times 10^5$ K, the *Chandra* non-detection of PS1-10jh places an upper limit on the bolometric luminosity of such a blackbody component of $\sim 10^{42}$ ergs s^{-1}, below the luminosities of 10^{42-44} ergs s^{-1} of the X-ray TDE candidates. However, the blackbody temperatures of the X-ray TDE candidates are hotter than expected for a TDE from basic theoretical arguments, and correspond to effective radii smaller than the Schwarzschild radius of their respective black holes. A lower effective temperature of $\lesssim 2.5 \times 10^5$ K, and thus a non-detection in the hard X-rays, is actually in better agreement with theoretical expectations for thermal emission from radii ranging from the innermost stable circular orbit ($R_{\rm ISCO}$) to the tidal disruption radius of the central black hole ($R_{\rm T}$). Furthermore, it would not be surprising if TDE candidates selected from X-ray surveys were more X-ray bright than those selected using other methods.

5 Nature of the Flare

The persistence of the hot blackbody emission up to 375 rest-frame days after the peak definitively excludes a supernova (SN) origin. Although core-collapse SNe are hot at early times ($\sim 10^4$ K), they quickly cool through expansion and radiation to ~ 6000 K by a month after explosion (i.e., Type II SNe[34,42,43], Type Ibc SNe[44], Ultraluminous SNe[45,46]). The lack of recent star-formation in the host galaxy also disfavors a core-collapse SN with a massive progenitor star with a short lifetime. The host galaxy is undetected in a deep coadd of all the *GALEX* TDS epochs in 2009 in the $FUV(\lambda_{\rm eff} = 153.9$ nm) with $t_{\rm exp} = 14.9$ ks and NUV with $t_{\rm exp} = 43.2$ ks, with 3σ upper limits of $FUV > 25.1$ mag and $NUV > 25.6$ mag. The upper limit on the NUV flux density corresponds to an upper limit on the star-formation rate[47] in the host galaxy of $< 0.022 M_\odot$ yr^{-1} after correcting for Galactic extinction.

The upper limit to the X-ray to UV luminosity density ratio $260 - 270$ rest-frame days from the peak is 20 times lower than observed in broad-lined AGNs of a comparable NUV luminosity[28], and argues strongly against an association of the flare with an AGN. Furthermore, the extreme amplitude of the flare of > 6.4 mag is most likely caused by a true transient event, and not from a fluctuation of unobscured accretion activity.

The amplitude of the flare could be explained by a change in the line-of-sight extinction toward the nucleus of the galaxy of $\Delta(N_H) = 5 \times 10^{21}$ cm^{-2}. However, in order to obscure the AGN hard X-ray emission during the flare, assuming a standard intrinsic α_{ox}, one requires $N_H \sim 10^{24}$ cm^{-2}. With such a high column density, for a standard gas-to-dust ratio the UV and optical extinction would be extremely large ($E(B - V) \sim 180$ mag), and no UV and optical flare from the nucleus would be observable.

X-ray bright optically normal galaxies (XBONGs) have been observed which show strong X-ray emission characteristic of an unobscured AGN, but with no optical emission lines characteristic of AGN activity. This scenario has been explained by an AGN with a unobscured nucleus whose optical nuclear emission lines are diluted by a strong stellar continuum[48]. These sources share the property with PS1-10jh in the lack of a standard AGN emission-line spectrum, however the detection of broad He II emission in PS1-10jh indicates that its optical nuclear spectrum is neither diluted nor absorbed.

6 Light Curve Fits to Tidal Disruption Accretion Rate Models

The index n of the power-law decay, $\dot{M} \propto (t/t_{\mathrm{min}})^{-n}$, is sensitive to mode of the accretion. For super-Eddington accretion rates, a radiation supported outflow expands with a receding photosphere[21], resulting in a brief outburst that peaks at $\sim 10 (M_{\mathrm{BH}}/10^6 M_\odot)^{-1/8} (R_{\mathrm{T}}/R_{\mathrm{p}})^{-9/8} m_\star r_\star^{6/8}$ d, and then declines in luminosity as $n = 5/9$. Emission on the Rayleigh-Jeans tail ($L_\nu \propto T$) of the hot outflow declines as $n = 35/36$. This power-law index can be fitted to the decay of PS1-10jh, but with $t_{\mathrm{min}} = 9 \pm 3$ rest-frame days, which is incompatible with the observed rise-time of the flare of > 35 rest-frame days.

For sub-Eddington accretion rates, the luminosity should follow the decline of the mass-return rate, which depends on the internal structure of the star at early times, but approaches an $n = 5/3$ power-law after a few times t_{min} for all stellar types. For $L = 4\pi R_{\mathrm{BB}}^2 \sigma T_{\mathrm{BB}}^4$, if $L \propto \dot{M} \propto (t/t_{\mathrm{min}})^{-5/3}$, then on the Rayleigh-Jeans tail, for a fixed R_{BB} one expects an $n = 5/12$ decay[21,49]. Our NUV and optical photometry of PS1-10jh are on the Rayleigh-Jeans tail of the $\gtrsim 3 \times 10^4$ K blackbody, yet we see a decline that follows the mass-return rate, with no indication of a shallower decline due to cooling of the emission. We also do not observe any evolution in the UV and optical SED that would indicate cooling over time.

13

A possible explanation for both the constant shape of the UV and optical SED and the linear scaling of the UV and optical light curve with the predicted bolometric luminosity evolution of the TDE, is that the UV and optical continuum is a "pseudo-continuum" whose shape is determined by atomic reprocessing. In such a scenario, the UV and optical SED shape remains fixed even if the photoionising continuum is cooling with time (its shape is determined by a velocity-blurred reflection spectrum and not the temperature of the photoionising continuum), and the UV and optical light follows the decay of the bolometric luminosity since it is the result of the reflection, absorption, and re-emission of the photoionising continuum. This explanation implies that the expected very hot $\approx 10^5$ K blackbody photoionising continuum is present in the unseen EUV region, but is masked in the observed UV and optical region by reprocessing. This model has also been invoked for normal AGNs to explain their low apparent thermal UV and optical continuum temperature (the Big Blue Bump)[22].

The rise and decay of PS1-10jh is well constrained by the PS1 photometry, and enables us to determine the polytropic exponent (γ) of the star disrupted. Figure S8 shows the fit to the g_{P1} light curve for models[20] with $\gamma = 1.4, 1.5, 5/3$, and 1.8. The data are in best agreement with the $\gamma = 5/3$ model. The derived parameters from the fits are stretch factors in time of $1.25, 1.09, 1.40$, and 1.77, respectively, and a time delay between the time of disruption and the peak of the flare of $56, 58, 78$, and 98, respectively. Without the constraints from the rise *and* decay of the light curve, the values for the stretch factor and the time of disruption can vary widely.

7   He Abundance and Internal Extinction

The He/H ratio is derived from $f(\text{He II}\lambda 4686)/f(\text{H}\alpha) = \frac{n(\text{He}^+)\alpha^{eff}_{\lambda 4686}h\nu_{\lambda 4686}}{n(\text{H}^0)\alpha^{eff}_{\text{H}\beta}(j_{\text{H}\alpha}/j_{\text{H}\beta})h\nu_{\text{H}\beta}}$, where $j_{\text{H}\alpha}/j_{\text{H}\beta} = 3.1$ includes the effects of collisional excitation, $\alpha^{eff}_{\text{H}\beta} = 3.03 \times 10^{-14}$ cm^3 s^{-1} and $\alpha^{eff}_{\lambda 4686} = 3.72 \times 10^{-13}$ for a gas temperature of $T = 1 \times 10^4$ K typical of nebular gas and the broad-line region of an AGN. The 3σ upper limit measured from the noise in the continuum of $\text{H}\alpha/\text{He II}\lambda 4686 < 0.2$ implies a He abundance of $n(\text{He}^+)/n(\text{H}^0) > 1.2$, which corresponds to a hydrogen mass fraction of $X = \frac{n_H}{n_H + 4n_{He}} < 0.2$. Since the number density of the unbound debris is high[21], $n \sim 3 \times 10^{13} M_6^{1/6} \beta^{-5} m_\star^{-2/3} r_\star^{3/2} (t/36 \text{ d})^{-3}$ cm^{-3}, the recombination time is short compared to the flare timescale, $\tau_{rec} = (n_e \alpha_B)^{-1} \sim (n\frac{1+2[n(\text{H}^0)/n(\text{He}^+)]}{1+n(\text{H}^0)/n(\text{He}^+)}\alpha_B)^{-1} \approx 0.08(\frac{t}{36\text{d}})^3$ sec, and we can assume that the gas reaches photoionization equilibrium instantaneously. We derive the internal extinction from $E(B - V)_{\text{int}} = \frac{\log(R_{\text{obs}}/R_{\text{int}})}{-0.4[k(\lambda 3203) - k(\lambda 4686)]} < 0.08$ mag, where R_{obs} and R_{int} are the observed and intrinsic He II $\lambda 3203/\lambda 4686$ ratios, and we use $R_{\text{obs}} = 0.5 \pm 0.1$ and $R_{\text{int}} = 0.45$, and an extinction law[50] with $k(\lambda 3203) - k(\lambda 4686) = 1.555$.
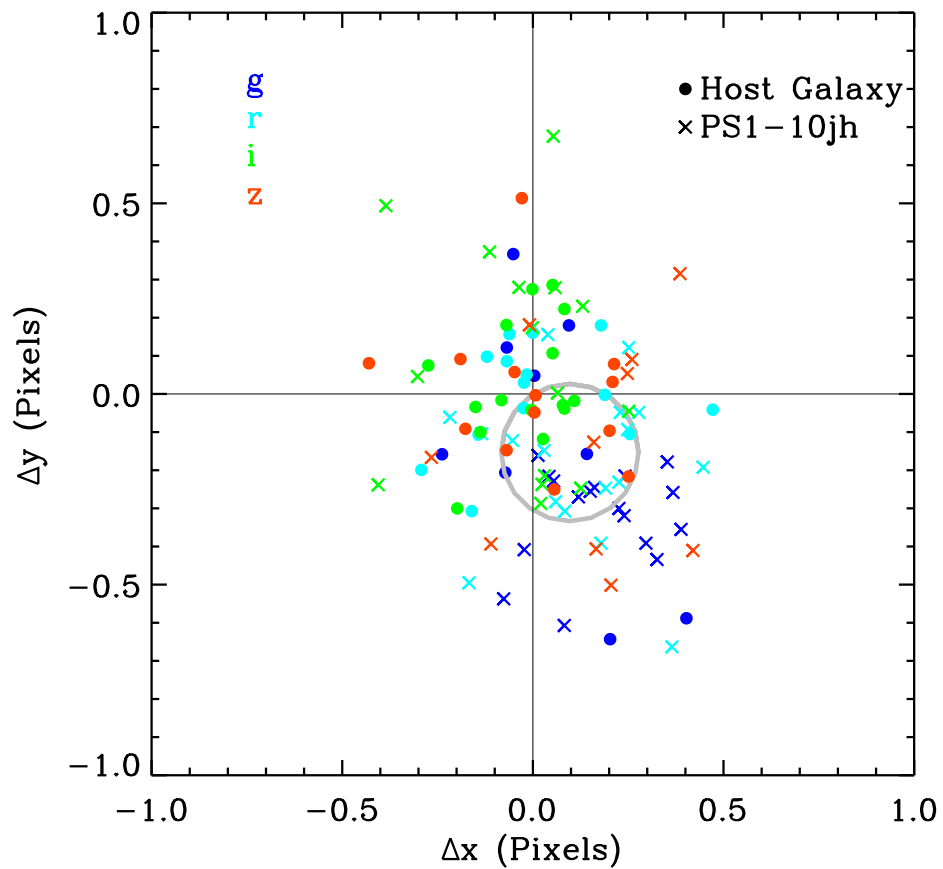
Figure 4

Offset of PS1-10jh from the mean x and y position of the host galaxy centroid measured in the nightly stacked images before the event. Solid points show the centroid of the host galaxy before the event, and X symbols show the centroid of PS1-10jh, in each of the 4 PS1 bands. Thick gray circle shows the mean offset and 3σ error of PS1-10jh from the host galaxy centroid.
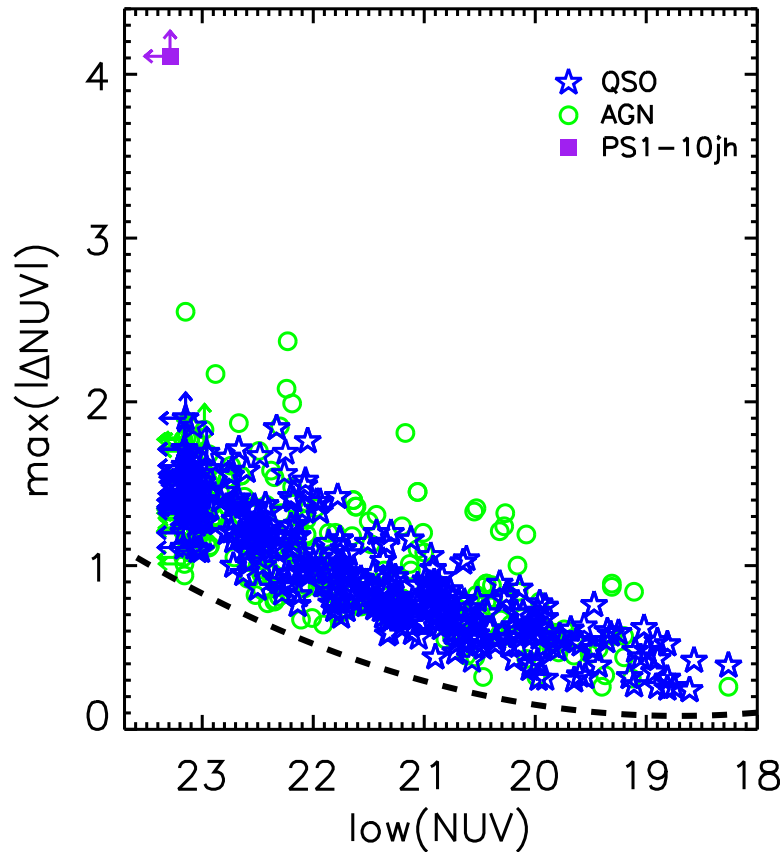
Figure 5

Maximum amplitude of NUV variability for quasars (blue stars) and active galactic nuclei (green circles) between individual epochs in the *GALEX* Time Domain Survey. Dashed line shows the median 5σ variability selection function used to select variable source in the *GALEX* Time Domain Survey fields. PS1-10jh (purple square) is a clear outlier from these populations, consistent with its NUV flare being a true transient, and not a fluctuation of ongoing accretion activity. When the pre-event epochs are coadded to a limiting magnitude of $NUV > 25.6$ mag, the peak amplitude of variability of PS1-10jh increases to > 6.4 mag.
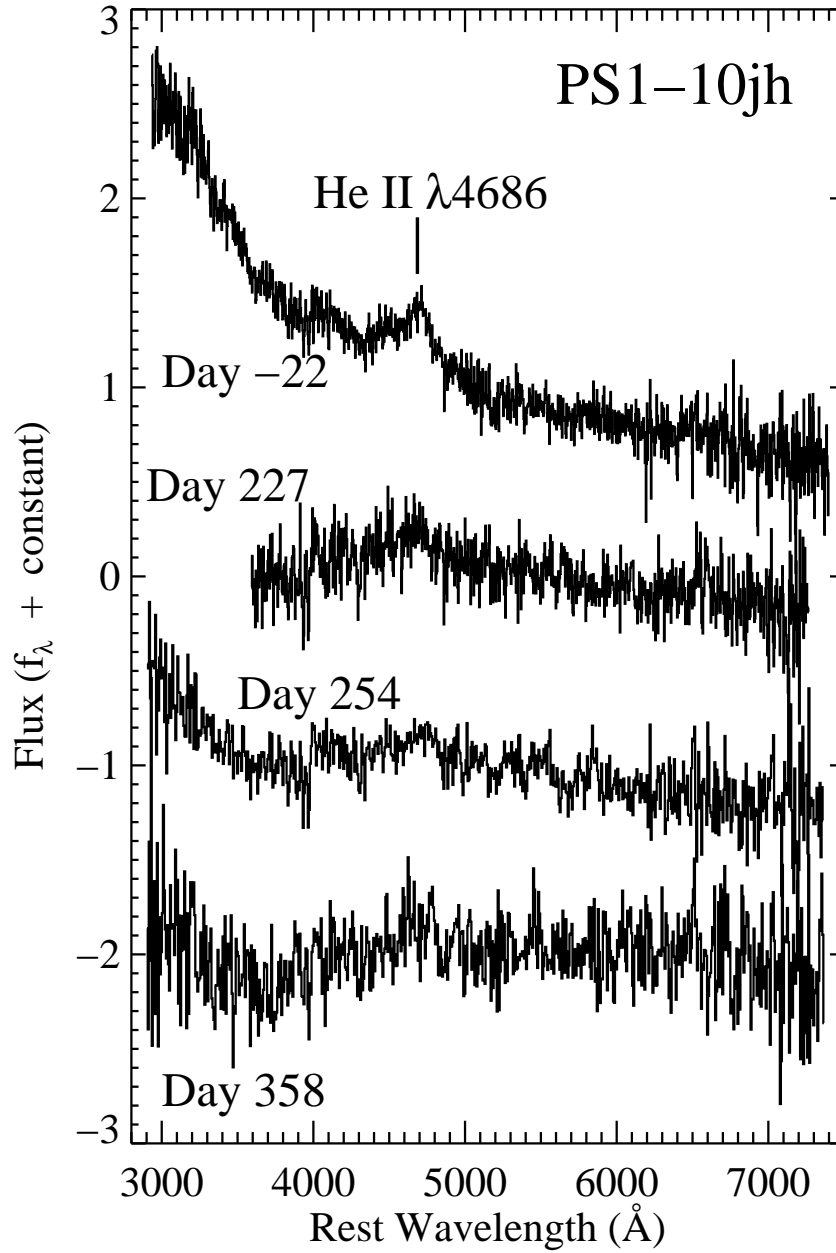
Figure 6
Series of MMT spectra of PS1-10jh in units of normalized flux density labeled by their phase in rest-frame days since the peak of the flare, plotted with vertical offsets for clarity. The wavelength of He II$\lambda 4686$ is labeled with a tick mark.

17
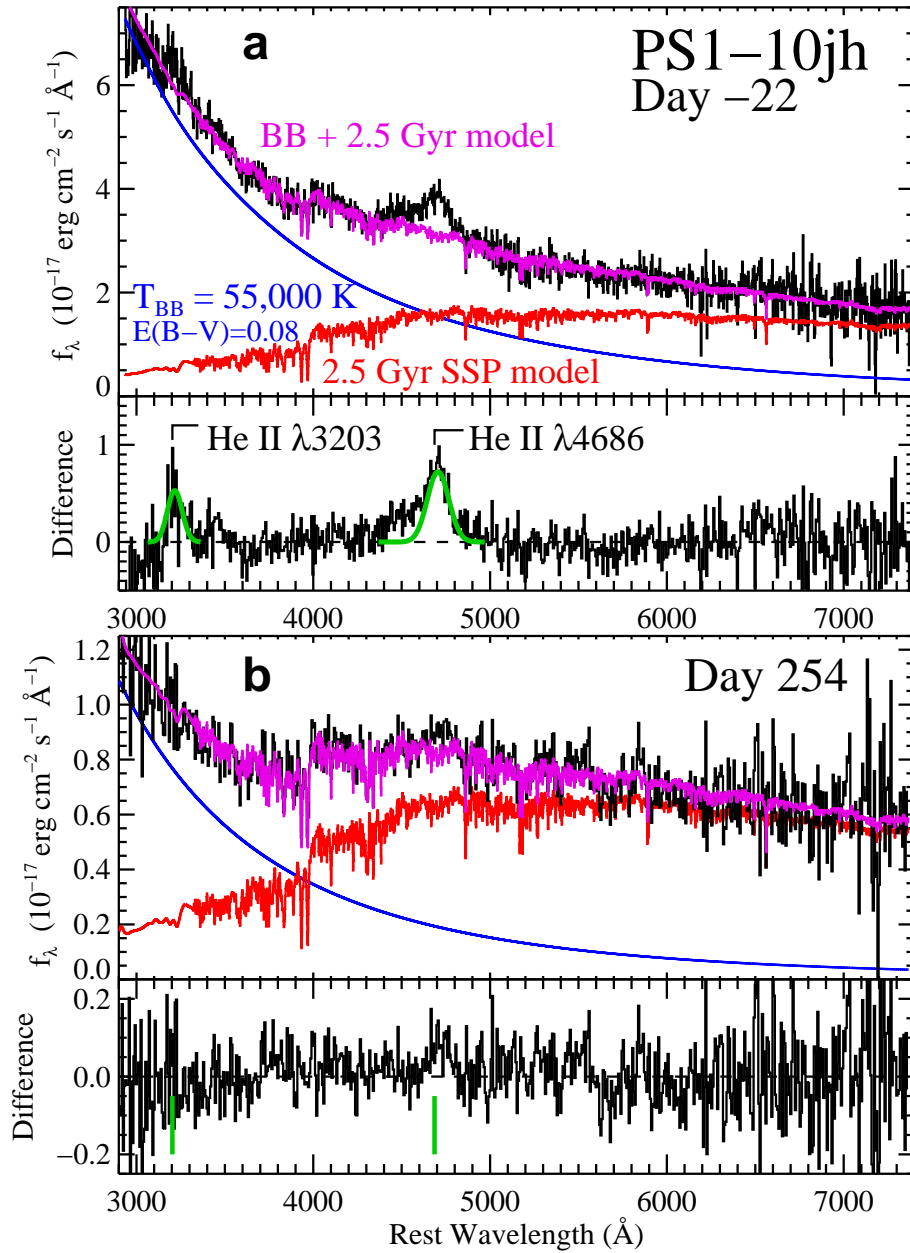
Figure 7
Same as Figure 1 in the paper, but dereddened for an internal extinction of $E(B - V) = 0.08$ mag, and the continuum fitted with a combination of the same galaxy template and a fading blackbody with $T_{\mathrm{BB}} \sim 5.5 \times 10^4 K$.
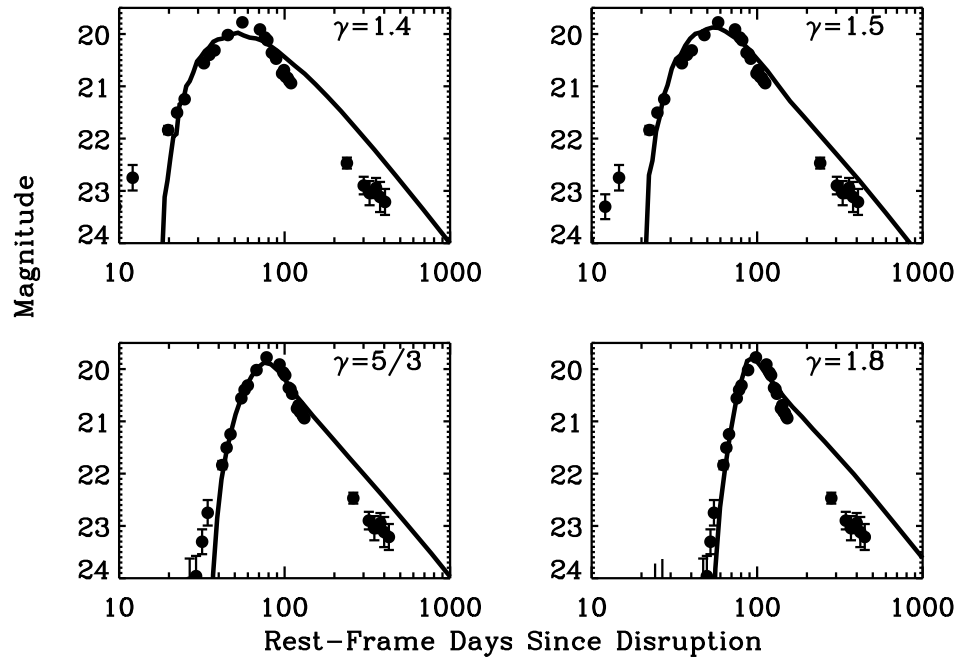
Figure 8
Fits of the g_{P1}-band light curve of PS1-10jh from -38 to 58 rest-frame days from the peak to models for the mass accretion rate of tidally disrupted stars of different polytropic exponent γ.

Table S1: Pan-STARRS1 Medium Deep Survey Observations

UT Date			Phase	Filter	Mag	σ
2009	May	28.48	-350.40	g_{P1}	>23.90	
2009	May	31.43	-347.88	g_{P1}	>23.89	
2009	Jun	14.45	-335.90	g_{P1}	>23.70	
2009	Jun	17.44	-333.34	g_{P1}	>23.79	
2009	Jun	20.42	-330.79	g_{P1}	>23.83	
2009	Jul	2.29	-320.64	g_{P1}	>23.62	
2009	Jul	17.30	-307.80	g_{P1}	>23.04	
2009	Sep	15.25	-256.55	g_{P1}	>23.84	
2010	Apr	16.59	-74.15	g_{P1}	>23.72	
2010	Apr	19.58	-71.59	g_{P1}	>23.63	
2010	May	10.55	-53.66	g_{P1}	25.43	1.49
2010	May	13.53	-51.11	g_{P1}	24.09	0.46
2010	May	16.43	-48.64	g_{P1}	23.96	0.39
2010	May	19.43	-46.07	g_{P1}	23.30	0.24
2010	May	22.43	-43.50	g_{P1}	22.75	0.24
2010	May	31.45	-35.80	g_{P1}	21.84	0.08
2010	Jun	3.51	-33.17	g_{P1}	21.50	0.05
2010	Jun	6.42	-30.69	g_{P1}	21.25	0.03
2010	Jun	15.37	-23.04	g_{P1}	20.56	0.02
2010	Jun	18.33	-20.50	g_{P1}	20.40	0.02
2010	Jun	21.40	-17.88	g_{P1}	20.31	0.02
2010	Jun	30.44	-10.15	g_{P1}	20.02	0.01
2010	Jul	12.31	0.00	g_{P1}	19.78	0.01
2010	Jul	30.34	15.41	g_{P1}	19.91	0.01
2010	Aug	5.32	20.53	g_{P1}	20.07	0.01
2010	Aug	8.30	23.07	g_{P1}	20.12	0.01
2010	Aug	14.29	28.19	g_{P1}	20.36	0.02
2010	Aug	17.26	30.73	g_{P1}	20.38	0.02
2010	Aug	20.27	33.30	g_{P1}	20.47	0.02
2010	Aug	29.26	41.00	g_{P1}	20.75	0.02
2010	Sep	1.29	43.58	g_{P1}	20.69	0.02
2010	Sep	4.26	46.12	g_{P1}	20.82	0.02
2010	Sep	7.27	48.70	g_{P1}	20.84	0.02
2010	Sep	10.23	51.23	g_{P1}	20.90	0.03
2010	Sep	13.25	53.81	g_{P1}	20.94	0.03
2011	Feb	10.62	182.37	g_{P1}	22.47	0.10
2011	Apr	23.51	243.84	g_{P1}	23.03	0.20
2011	Apr	26.58	246.47	g_{P1}	22.77	0.13
2011	May	20.57	266.97	g_{P1}	23.10	0.29

20

2011	May	29.46	274.58	g_{P1}	22.99	0.16
2011	Jun	10.38	284.77	g_{P1}	25.83	5.98
2011	Jun	25.39	297.61	g_{P1}	22.75	0.14
2011	Jun	28.38	300.16	g_{P1}	23.09	0.28
2011	Jul	1.32	302.68	g_{P1}	23.20	0.19
2011	Jul	4.33	305.25	g_{P1}	22.74	0.12
2011	Jul	10.31	310.36	g_{P1}	22.74	0.19
2011	Jul	19.28	318.03	g_{P1}	23.28	0.21
2011	Jul	22.28	320.60	g_{P1}	23.54	0.38
2011	Jul	25.28	323.16	g_{P1}	22.96	0.16
2011	Jul	28.28	325.72	g_{P1}	22.49	0.10
2011	Jul	31.28	328.29	g_{P1}	22.81	0.14
2011	Aug	3.30	330.87	g_{P1}	23.04	0.16
2011	Aug	6.27	333.41	g_{P1}	24.08	0.60
2011	Aug	18.29	343.69	g_{P1}	22.96	0.15
2011	Aug	21.27	346.23	g_{P1}	23.07	0.16
2011	Aug	24.27	348.80	g_{P1}	23.14	0.18
2011	Aug	27.25	351.35	g_{P1}	22.87	0.20
2011	Aug	30.28	353.94	g_{P1}	24.01	0.43
2009	Apr	20.62	-382.77	r_{P1}	>23.35	
2009	Apr	29.61	-375.09	r_{P1}	>23.30	
2009	Apr	30.60	-374.24	r_{P1}	>23.34	
2009	May	2.59	-372.54	r_{P1}	>23.32	
2009	May	22.52	-355.50	r_{P1}	>23.37	
2009	Jun	11.46	-338.45	r_{P1}	>23.26	
2009	Jun	14.46	-335.89	r_{P1}	>23.20	
2009	Jun	17.46	-333.32	r_{P1}	>23.06	
2009	Jun	20.43	-330.78	r_{P1}	>23.31	
2009	Jul	2.31	-320.63	r_{P1}	>23.29	
2009	Sep	15.26	-256.54	r_{P1}	>23.32	
2010	Apr	19.60	-71.58	r_{P1}	>23.20	
2010	May	16.44	-48.63	r_{P1}	24.21	0.81
2010	May	19.45	-46.06	r_{P1}	23.34	0.39
2010	May	22.45	-43.49	r_{P1}	22.71	0.29
2010	May	31.46	-35.78	r_{P1}	22.46	0.17
2010	Jun	3.53	-33.16	r_{P1}	21.80	0.09
2010	Jun	6.44	-30.67	r_{P1}	21.50	0.07
2010	Jun	15.38	-23.03	r_{P1}	20.94	0.04
2010	Jun	18.32	-20.51	r_{P1}	20.69	0.03
2010	Jun	21.41	-17.87	r_{P1}	20.63	0.03
2010	Jun	30.45	-10.14	r_{P1}	20.32	0.03
2010	Jul	12.30	-0.01	r_{P1}	20.12	0.02

2010	Jul	30.35	15.42	r_{P1}	20.23	0.02
2010	Aug	5.31	20.52	r_{P1}	20.36	0.02
2010	Aug	8.32	23.09	r_{P1}	20.46	0.03
2010	Aug	14.30	28.21	r_{P1}	20.69	0.05
2010	Aug	17.27	30.75	r_{P1}	20.70	0.04
2010	Aug	20.28	33.31	r_{P1}	20.72	0.04
2010	Aug	29.27	41.01	r_{P1}	21.08	0.05
2010	Sep	1.27	43.57	r_{P1}	21.10	0.05
2010	Sep	4.27	46.13	r_{P1}	21.15	0.05
2010	Sep	7.29	48.71	r_{P1}	21.18	0.05
2010	Sep	10.24	51.24	r_{P1}	21.22	0.05
2010	Sep	13.27	53.82	r_{P1}	21.38	0.07
2011	Feb	10.63	182.38	r_{P1}	22.47	0.17
2011	Apr	23.52	243.85	r_{P1}	23.01	0.27
2011	Apr	26.59	246.48	r_{P1}	23.58	0.46
2011	May	20.58	266.98	r_{P1}	23.41	0.47
2011	May	29.48	274.59	r_{P1}	23.57	0.45
2011	Jun	10.39	284.78	r_{P1}	22.78	0.27
2011	Jun	25.41	297.62	r_{P1}	23.04	0.31
2011	Jun	28.39	300.17	r_{P1}	24.37	1.52
2011	Jul	1.34	302.69	r_{P1}	23.48	0.43
2011	Jul	4.34	305.26	r_{P1}	23.25	0.33
2011	Jul	10.32	310.37	r_{P1}	24.01	0.76
2011	Jul	19.29	318.04	r_{P1}	23.01	0.28
2011	Jul	22.29	320.61	r_{P1}	23.39	0.54
2011	Jul	25.30	323.17	r_{P1}	23.60	0.46
2011	Jul	28.29	325.74	r_{P1}	23.10	0.29
2011	Jul	31.29	328.30	r_{P1}	23.44	0.42
2011	Aug	3.32	330.89	r_{P1}	23.53	0.43
2011	Aug	6.28	333.42	r_{P1}	24.59	1.24
2011	Aug	18.30	343.70	r_{P1}	23.89	0.60
2011	Aug	21.28	346.25	r_{P1}	23.41	0.38
2011	Aug	24.28	348.81	r_{P1}	23.46	0.40
2011	Aug	30.29	353.95	r_{P1}	24.19	0.80
2009	Apr	19.55	-383.69	i_{P1}	>22.65	
2009	Apr	20.59	-382.80	i_{P1}	>22.93	
2009	May	1.61	-373.38	i_{P1}	>22.90	
2009	May	2.55	-372.57	i_{P1}	>22.84	
2009	Jun	2.42	-346.18	i_{P1}	>22.94	
2009	Jun	3.47	-345.28	i_{P1}	>22.91	
2009	Jun	15.37	-335.11	i_{P1}	>22.97	
2009	Jun	18.40	-332.52	i_{P1}	>22.93	

2009	Jun	30.36	-322.29	i_{P1}	>22.95	
2009	Jul	3.32	-319.76	i_{P1}	>22.84	
2009	Sep	1.25	-268.52	i_{P1}	>22.86	
2009	Sep	19.24	-253.14	i_{P1}	>22.88	
2010	Apr	2.54	-86.16	i_{P1}	>22.91	
2010	Apr	14.59	-75.85	i_{P1}	>22.93	
2010	May	8.59	-55.34	i_{P1}	>22.94	
2010	May	11.61	-52.76	i_{P1}	24.45	1.44
2010	Jun	1.41	-34.97	i_{P1}	22.59	0.26
2010	Jun	16.50	-22.07	i_{P1}	21.00	0.06
2010	Jun	19.33	-19.65	i_{P1}	20.85	0.05
2010	Jul	1.35	-9.37	i_{P1}	20.48	0.04
2010	Jul	31.30	16.23	i_{P1}	20.35	0.03
2010	Aug	3.35	18.84	i_{P1}	20.47	0.04
2010	Aug	6.33	21.39	i_{P1}	20.51	0.04
2010	Aug	9.28	23.91	i_{P1}	20.52	0.04
2010	Aug	15.28	29.04	i_{P1}	20.69	0.04
2010	Aug	30.29	41.88	i_{P1}	21.27	0.08
2010	Sep	2.27	44.42	i_{P1}	21.14	0.07
2010	Sep	5.27	46.98	i_{P1}	21.24	0.07
2010	Sep	8.26	49.55	i_{P1}	21.31	0.08
2010	Sep	11.26	52.11	i_{P1}	21.43	0.09
2010	Sep	14.25	54.66	i_{P1}	21.47	0.09
2010	Sep	17.23	57.21	i_{P1}	21.52	0.10
2011	Feb	23.63	193.50	i_{P1}	23.45	0.83
2011	Apr	21.51	242.13	i_{P1}	23.05	0.40
2011	Apr	24.58	244.76	i_{P1}	23.18	0.45
2011	Apr	27.55	247.30	i_{P1}	23.72	0.74
2011	May	12.43	260.01	i_{P1}	23.99	1.57
2011	May	21.52	267.79	i_{P1}	23.88	0.88
2011	May	27.43	272.84	i_{P1}	24.07	1.04
2011	May	30.49	275.46	i_{P1}	23.67	0.70
2011	Jun	2.40	277.95	i_{P1}	23.92	0.87
2011	Jun	11.35	285.60	i_{P1}	23.18	0.45
2011	Jun	26.39	298.46	i_{P1}	23.12	0.49
2011	Jun	29.46	301.08	i_{P1}	23.66	0.70
2011	Jul	2.32	303.53	i_{P1}	23.44	0.57
2011	Jul	5.34	306.11	i_{P1}	23.47	0.58
2011	Jul	11.29	311.20	i_{P1}	23.60	0.65
2011	Jul	20.34	318.93	i_{P1}	24.10	1.04
2011	Jul	23.29	321.45	i_{P1}	23.47	0.62
2011	Jul	26.29	324.02	i_{P1}	23.82	0.79

2011	Jul	29.32	326.61	i_{P1}	23.74	0.78
2011	Aug	1.27	329.14	i_{P1}	23.39	0.53
2011	Aug	4.27	331.70	i_{P1}	23.38	0.53
2011	Aug	16.28	341.97	i_{P1}	23.67	0.71
2011	Aug	19.31	344.56	i_{P1}	23.22	0.47
2011	Aug	22.27	347.09	i_{P1}	23.67	0.70
2011	Aug	28.26	352.21	i_{P1}	24.11	1.04
2011	Aug	31.27	354.79	i_{P1}	23.13	0.43
2011	Sep	3.25	357.33	i_{P1}	24.06	1.04
2009	May	5.46	-370.08	z_{P1}	>22.97	
2009	May	6.55	-369.15	z_{P1}	>22.82	
2009	Jun	13.42	-336.78	z_{P1}	>23.04	
2009	Jun	16.43	-334.20	z_{P1}	>22.88	
2009	Jun	25.39	-326.54	z_{P1}	>22.97	
2009	Jun	28.37	-324.00	z_{P1}	>23.02	
2009	Jul	4.30	-318.93	z_{P1}	>22.97	
2009	Jul	22.39	-303.45	z_{P1}	>22.64	
2009	Sep	20.24	-252.29	z_{P1}	>22.19	
2009	Sep	29.22	-244.60	z_{P1}	>23.02	
2010	Apr	9.62	-80.11	z_{P1}	>22.90	
2010	Apr	12.61	-77.55	z_{P1}	>23.11	
2010	Apr	18.59	-72.44	z_{P1}	>23.06	
2010	May	9.52	-54.55	z_{P1}	>22.96	
2010	May	21.51	-44.29	z_{P1}	24.88	2.03
2010	Jun	5.46	-31.50	z_{P1}	21.82	0.11
2010	Jun	11.55	-26.30	z_{P1}	21.51	0.10
2010	Jun	14.37	-23.89	z_{P1}	21.28	0.07
2010	Jun	17.40	-21.30	z_{P1}	21.47	0.10
2010	Jun	20.31	-18.81	z_{P1}	20.97	0.05
2010	Jun	29.39	-11.04	z_{P1}	20.64	0.04
2010	Jul	2.29	-8.57	z_{P1}	20.67	0.04
2010	Jul	29.39	14.61	z_{P1}	20.62	0.04
2010	Aug	1.34	17.13	z_{P1}	20.57	0.04
2010	Aug	4.38	19.72	z_{P1}	20.64	0.04
2010	Aug	16.30	29.92	z_{P1}	20.95	0.05
2010	Aug	19.25	32.44	z_{P1}	21.02	0.05
2010	Aug	31.24	42.69	z_{P1}	21.13	0.06
2010	Sep	3.24	45.25	z_{P1}	21.32	0.07
2010	Sep	6.24	47.82	z_{P1}	21.47	0.09
2010	Sep	9.23	50.38	z_{P1}	21.39	0.08
2010	Sep	12.26	52.96	z_{P1}	21.25	0.10
2010	Sep	15.25	55.52	z_{P1}	21.60	0.10

2010	Sep	18.23	58.07	z_{P1}	21.79	0.14
2011	Feb	3.65	176.42	z_{P1}	22.66	0.23
2011	Apr	22.56	243.03	z_{P1}	22.66	0.23
2011	Apr	25.55	245.59	z_{P1}	22.17	0.43
2011	May	13.46	260.90	z_{P1}	24.88	7.52
2011	Jun	12.45	286.54	z_{P1}	23.58	0.66
2011	Jun	24.46	296.81	z_{P1}	22.76	0.27
2011	Jun	30.32	301.82	z_{P1}	22.91	0.30
2011	Jul	3.34	304.40	z_{P1}	23.06	0.34
2011	Jul	6.31	306.94	z_{P1}	22.61	0.22
2011	Jul	9.31	309.51	z_{P1}	23.14	0.40
2011	Jul	12.31	312.07	z_{P1}	22.70	0.24
2011	Jul	18.30	317.20	z_{P1}	23.48	0.53
2011	Jul	21.29	319.74	z_{P1}	24.10	0.93
2011	Jul	24.27	322.29	z_{P1}	22.63	0.30
2011	Jul	27.26	324.85	z_{P1}	22.77	0.25
2011	Aug	2.26	329.98	z_{P1}	22.93	0.28
2011	Aug	5.26	332.55	z_{P1}	23.08	0.39
2011	Aug	17.28	342.82	z_{P1}	23.04	0.32
2011	Aug	20.31	345.42	z_{P1}	23.15	0.37
2011	Aug	23.27	347.95	z_{P1}	23.34	0.42
2011	Aug	29.25	353.06	z_{P1}	23.89	0.82
2011	Sep	1.24	355.62	z_{P1}	24.07	0.93

Table S2: *GALEX* Time Domain Survey Observations

UT Date			Phase[1]	Filter	Mag	σ
2009	May	9.52	-366.62	*NUV*	>23.72	
2009	May	11.98	-364.51	*NUV*	>23.74	
2009	May	13.90	-362.87	*NUV*	>23.77	
2009	May	15.82	-361.23	*NUV*	>23.80	
2009	May	17.80	-359.53	*NUV*	>23.84	
2009	Jun	21.52	-329.85	*NUV*	>23.80	
2009	Jun	23.57	-328.10	*NUV*	>23.75	
2009	Jun	25.42	-326.51	*NUV*	>23.70	
2009	Jun	27.48	-324.76	*NUV*	>23.64	
2009	Jun	29.60	-322.94	*NUV*	>23.63	
2009	Jul	1.66	-321.18	*NUV*	>23.68	
2010	May	3.77	-59.46	*NUV*	>23.77	
2010	May	7.74	-56.06	*NUV*	>23.82	
2010	May	9.86	-54.25	*NUV*	>23.85	
2010	Jun	17.68	-21.06	*NUV*	19.47	0.07
2010	Jun	19.95	-19.12	*NUV*	19.41	0.08
2010	Jun	23.57	-16.02	*NUV*	19.18	0.04
2011	Apr	21.84	242.41	*NUV*	21.99	0.13
2011	Apr	23.89	244.17	*NUV*	21.79	0.12
2011	Apr	25.81	245.81	*NUV*	21.70	0.12
2011	May	8.40	256.57	*NUV*	21.88	0.11
2011	May	10.39	258.27	*NUV*	21.85	0.12
2011	May	12.37	259.97	*NUV*	22.01	0.16
2011	Jun	6.56	281.51	*NUV*	22.07	0.16
2011	Jun	10.68	285.02	*NUV*	22.48	0.16

[1]In rest-frame days after the peak on 2010 July 12.31 UT

Table S3: Log of Spectroscopic Observations

Phase[2]	UT Midpoint	Instrument	Exp. Time (s)	Wavelength Range (Å)	Resolution (Å)	Airmass	Slit P.A. (deg)	Parall. Angle (deg)
-22	2010-06-16.33	MMT/Blue Channel	1800	$3433 - 8655$	5.5	1.16	131.6	130.9
227	2011-04-03.48	MMT/Hectospec	3060	$3700 - 9150$	5.0	1.08	Fiber	
254	2011-05-05.47	MMT/Blue Channel	1200	$3396 - 8616$	5.5	1.21	117.7	117.6
255	2011-05-06.42	MMT/Blue Channel	1800	$3396 - 8616$	5.5	1.12	141.7	141.5
358	2011-09-04.23	MMT/Blue Channel	1500	$3394 - 8622$	5.5	1.78	83.8	83.8

[2]In rest-frame days after the peak on 2010 July 12.31 UT

1. Rees, M. J. Tidal disruption of stars by black holes of 10 to the 6th-10 to the 8th solar masses in nearby galaxies. Nature **333**, 523–528 (1988).

2. Komossa, S. & Bade, N. The giant X-ray outbursts in NGC 5905 and IC 3599:() hfill Follow-up observations and outburst scenarios. Astron. Astrophys. **343**, 775–787 (1999). `arXiv:astro-ph/9901141`.

3. Komossa, S. *et al.* A Huge Drop in the X-Ray Luminosity of the Nonactive Galaxy RX J1242.6-1119A, and the First Postflare Spectrum: Testing the Tidal Disruption Scenario. Astrophys. J. **603**, L17–L20 (2004). `arXiv:astro-ph/0402468`.

4. Esquej, P. *et al.* Evolution of tidal disruption candidates discovered by XMM-Newton. Astron. Astrophys. **489**, 543–554 (2008). `0807.4452`.

5. Gezari, S. *et al.* Luminous Thermal Flares from Quiescent Supermassive Black Holes. Astrophys. J. **698**, 1367–1379 (2009). `0904.1596`.

6. van Velzen, S. *et al.* Optical Discovery of Probable Stellar Tidal Disruption Flares. Astrophys. J. **741**, 73–96 (2011). `1009.1627`.

7. Bloom, J. S. *et al.* A Possible Relativistic Jetted Outburst from a Massive Black Hole Fed by a Tidally Disrupted Star. *Science* **333**, 203–206 (2011). `1104.3257`.

8. Burrows, D. N. *et al.* Relativistic jet activity from the tidal disruption of a star by a massive black hole. Nature **476**, 421–424 (2011). `1104.4787`.

9. Zauderer, B. A. *et al.* Birth of a relativistic outflow in the unusual γ-ray transient Swift J164449.3+573451. Nature **476**, 425–428 (2011). `1106.3568`.

10. Cenko, S. B. *et al.* Swift J2058.4+0516: Discovery of a Possible Second Relativistic Tidal Disruption Flare. *ArXiv e-prints* (2011). `1107.5307`.

11. Phinney, E. S. Manifestations of a Massive Black Hole in the Galactic Center. In M. Morris (ed.) *The Center of the Galaxy*, vol. 136 of *IAU Symposium*, 543–553 (1989).

12. Evans, C. R. & Kochanek, C. S. The tidal disruption of a star by a massive black hole. Astrophys. J. **346**, L13–L16 (1989).

13. Ulmer, A. Flares from the Tidal Disruption of Stars by Massive Black Holes. Astrophys. J. **514**, 180–187 (1999).

14. Kaiser, N. *et al.* The Pan-STARRS wide-field optical/NIR imaging survey. In *Society of Photo-Optical Instrumentation Engineers (SPIE) Conference Series*, vol. 7733 of *Society of Photo-Optical Instrumentation Engineers (SPIE) Conference Series* (2010).

15. Martin, D. C. *et al.* The Galaxy Evolution Explorer: A Space Ultraviolet Survey Mission. Astrophys. J. **619**, L1–L6 (2005). `arXiv:astro-ph/0411302`.

16. Aihara, H. *et al.* The Eighth Data Release of the Sloan Digital Sky Survey: First Data from SDSS-III. Astrophys. J. Sup. **193**, 29–45 (2011). `1101.1559`.

17. Lawrence, A. *et al.* The UKIRT Infrared Deep Sky Survey (UKIDSS). Mon. Not. R. Astron. Soc. **379**, 1599–1617 (2007). `arXiv:astro-ph/0604426`.

18. Blanton, M. R. & Roweis, S. K-Corrections and Filter Transformations in the Ultraviolet, Optical, and Near-Infrared. Astron. J. **133**, 734–754 (2007). `arXiv:astro-ph/0606170`.

19. Häring, N. & Rix, H.-W. On the Black Hole Mass-Bulge Mass Relation. Astrophys. J. **604**, L89–L92 (2004). `arXiv:astro-ph/0402376`.

20. Lodato, G., King, A. R. & Pringle, J. E. Stellar disruption by a supermassive black hole: is the light curve really proportional to $t^{-5/3}$? Mon. Not. R. Astron. Soc. **392**, 332–340 (2009). `0810.1288`.

21. Strubbe, L. E. & Quataert, E. Optical flares from the tidal disruption of stars by massive black holes. Mon. Not. R. Astron. Soc. **400**, 2070–2084 (2009). `0905.3735`.

22. Lawrence, A. The UV peak in Active Galactic Nuclei : a false continuum from blurred reflection ? *ArXiv e-prints* (2011). `1110.0854`.

23. Loeb, A. & Ulmer, A. Optical Appearance of the Debris of a Star Disrupted by a Massive Black Hole. Astrophys. J. **489**, 573–578 (1997). `arXiv:astro-ph/9703079`.

24. Davies, M. B. & King, A. The Stars of the Galactic Center. Astrophys. J. **624**, L25–L27 (2005). `arXiv:astro-ph/0503441`.

25. Kobayashi, S., Laguna, P., Phinney, E. S. & Mészáros, P. Gravitational Waves and X-Ray Signals from Stellar Disruption by a Massive Black Hole. Astrophys. J. **615**, 855–865 (2004). `arXiv:astro-ph/0404173`.

26. Maxted, P. F. L. *et al.* Discovery of a stripped red giant core in a bright eclipsing binary system. Mon. Not. R. Astron. Soc. **418**, 1156–1164 (2011). `1107.4986`.

27. Ayal, S., Livio, M. & Piran, T. Tidal Disruption of a Solar-Type Star by a Supermassive Black Hole. Astrophys. J. **545**, 772–780 (2000). `arXiv:astro-ph/0002499`.

28. Steffen, A. T. *et al.* The X-Ray-to-Optical Properties of Optically Selected Active Galaxies over Wide Luminosity and Redshift Ranges. Astron. J. **131**, 2826–2842 (2006). `arXiv:astro-ph/0602407`.

29. Steele, I. A. *et al.* The Liverpool Telescope: performance and first results. In J. M. Oschmann Jr. (ed.) *Society of Photo-Optical Instrumentation Engineers (SPIE) Conference Series*, vol. 5489 of *Society of Photo-Optical Instrumentation Engineers (SPIE) Conference Series*, 679–692 (2004).

30. Magnier, E. The Pan-STARRS PS1 Image Processing Pipeline. In *The Advanced Maui Optical and Space Surveillance Technologies Conference* (2006).

31. Rest, A. *et al.* Testing LMC Microlensing Scenarios: The Discrimination Power of the SuperMACHO Microlensing Survey. Astrophys. J. **634**, 1103–1115 (2005). `arXiv:astro-ph/0509240`.

32. Magnier, E. Calibration of the Pan-STARRS 3π Survey. In C. Sterken (ed.) *The Future of Photometric, Spectrophotometric and Polarimetric Standardization*, vol. 364 of *Astronomical Society of the Pacific Conference Series*, 153–+ (2007).

33. Magnier, E. A., Liu, M., Monet, D. G. & Chambers, K. C. The extended solar neighborhood: precision astrometry from the Pan-STARRS 1 3π Survey. In W. J. Jin, I. Platais, & M. A. C. Perryman (ed.) *IAU Symposium*, vol. 248 of *IAU Symposium*, 553–559 (2008).

34. Gezari, S. *et al.* GALEX and Pan-STARRS1 Discovery of SN IIP 2010aq: The First Few Days After Shock Breakout in a Red Supergiant Star. Astrophys. J. **720**, L77–L81 (2010). `1007.4551`.

35. Morrissey, P. *et al.* The Calibration and Data Products of GALEX. Astrophys. J. Sup. **173**, 682–697 (2007).

36. Schmidt, G. D., Weymann, R. J. & Foltz, C. B. A moderate-resolution, high-throughput CCD channel for the Multiple Mirror Telescope spectrograph. Publ. Astron. Soc. Pac. **101**, 713–724 (1989).

37. Fabricant, D. *et al.* Hectospec, the MMT's 300 Optical Fiber-Fed Spectrograph. Publ. Astron. Soc. Pac. **117**, 1411–1434 (2005). `arXiv:astro-ph/0508554`.

38. Mink, D. J. *et al.* Automating Reduction of Multifiber Spectra from the MMT Hectospec and Hectochelle. In R. A. Shaw, F. Hill, & D. J. Bell (ed.) *Astronomical Data Analysis Software and Systems XVI*, vol. 376 of *Astronomical Society of the Pacific Conference Series*, 249–+ (2007).

39. Filippenko, A. V. The importance of atmospheric differential refraction in spectrophotometry. Publ. Astron. Soc. Pac. **94**, 715–721 (1982).

40. Tremonti, C. A. *et al.* The Origin of the Mass-Metallicity Relation: Insights from 53,000 Star-forming Galaxies in the Sloan Digital Sky Survey. Astrophys. J. **613**, 898–913 (2004). `arXiv:astro-ph/0405537`.

41. Weisskopf, M. C. *et al.* An Overview of the Performance and Scientific Results from the Chandra X-Ray Observatory. Publ. Astron. Soc. Pac. **114**, 1–24 (2002). `arXiv:astro-ph/0110308`.

42. Hamuy, M., Suntzeff, N. B., Gonzalez, R. & Martin, G. SN 1987A in the LMC - UBVRI photometry at Cerro Tololo. Astron. J. **95**, 63–83 (1988).

43. Dessart, L. *et al.* Using Quantitative Spectroscopic Analysis to Determine the Properties and Distances of Type II Plateau Supernovae: SN 2005cs and SN 2006bp. Astrophys. J. **675**, 644–669 (2008). `0711.1815`.

44. Soderberg, A. M. *et al.* An extremely luminous X-ray outburst at the birth of a supernova. Nature **453**, 469–474 (2008). `0802.1712`.

45. Gezari, S. *et al.* Discovery of the Ultra-Bright Type II-L Supernova 2008es. Astrophys. J. **690**, 1313–1321 (2009). `0808.2812`.

46. Chomiuk, L. *et al.* Pan-STARRS1 Discovery of Two Ultra-Luminous Supernovae at z ~ 0.9. *ArXiv e-prints* (2011). `1107.3552`.

47. Kennicutt, R. C., Jr. Star Formation in Galaxies Along the Hubble Sequence. Annu. Rev. Astron. Astr. **36**, 189–232 (1998). `arXiv:astro-ph/9807187`.

48. Georgantopoulos, I. & Georgakakis, A. X-ray bright optically inactive galaxies in XMM-Newton/Sloan Digital Sky Survey fields: more diluted than absorbed? Mon. Not. R. Astron. Soc. **358**, 131–138 (2005). `arXiv:astro-ph/0412335`.

49. Lodato, G. & Rossi, E. M. Multiband light curves of tidal disruption events. Mon. Not. R. Astron. Soc. **410**, 359–367 (2011). `1008.4589`.

50. Cardelli, J. A., Clayton, G. C. & Mathis, J. S. The relationship between infrared, optical, and ultraviolet extinction. Astrophys. J. **345**, 245–256 (1989).